Geostationary Lightning Mapper Flash Characteristics of Electrified Snowfall Events

Sebastian S. Harkema*

Department of Atmospheric Science, The University of Alabama in Huntsville, Huntsville, AL

Christopher J. Schultz and Emily B. Berndt

NASA Marshall Space Flight Center, Huntsville, AL

Phillip M. Bitzer

Department of Atmospheric Science, The University of Alabama in Huntsville, Huntsville, AL

Corresponding author address: Sebastian S. Harkema, Department of Atmospheric Science, The University of Alabama in Huntsville, 320 Sparkman Dr. NW, Huntsville, AL 35805

E-mail: sebastian.harkema@nasa.gov

Abstract

This study examines characteristics of lightning in snowfall events (i.e., thundersnow, TSSN) from the perspective of the Geostationary Lightning Mapper (GLM) and the National Environmental Satellite Data and Information Service (NESDIS) merged Snowfall Rate (mSFR) product. A thundersnow detection algorithm (TDA) was derived from the GLM and mSFR which resulted in a probability of detection (POD) of 66.7% when compared to the Meteorological Terminal Air Report (METAR) reports of TSSN. However, using the TDA an additional 2,175 lightning flashes within detected snowfall were identified that were not observed by the METAR reports, indicating that TSSN has been under reported in previous literature. TSSN flashes observed by GLM have mean flash areas, durations, and total optical energy outputs of 754 km^2, 402 ms, and 1,342 fJ, which are between the 50^{th} and 99^{th} percentile values for all flashes within the GLM field of view. A comparison with data from the National Lightning Detection Network (NLDN) indicated that the NLDN had at least one cloud or ground flash detection in 1,709 of the 2,214 flashes observed by GLM in snowfall. An average of 5.85 NLDN flashes were assigned to a single GLM flash when the NLDN flash data were constrained by the GLM flash duration and spatial footprint. Statistically significant ($p<0.01$) differences in flash area and flash energy were found between flashes that were observed by the NLDN and those that were not. Additionally, when GLM was combined with the NLDN, at least 11.1% of flashes involved a tall human-made object like an antenna or wind turbine.

1. Introduction

The Geostationary Lightning Mapper (GLM; Goodman et al. 2013; Rudlosky et al. 2019), onboard the Geostationary Operation Environmental Satellite – R (GOES-R; Schmit et al. 2005) Series satellites (now GOES-East and –West), provides unprecedented observations for lightning detection with a near-uniform storm-scale coverage and a spatial and temporal resolution of 8 km and 2 ms respectively (Goodman et al. 2013). The GLM provides characteristics of lightning occurrence, flash size, and flash radiance that can be applied in the detection of severe storms, lightning-initiated wildfires, and heavy snowfall rates in winter storms. Schultz et al. (2018) were the first to demonstrate the ability of GLM to identify lightning associated with snowfall (i.e., thundersnow, TSSN) for a lake-effect snow event in New York where lightning was detected in a winter environment in close proximity to tall man-made structures, thus providing evidence that GLM can detect lightning in winter environments on small scales and indicates promising results when utilized for TSSN and heavy-snowfall associated with mid-latitude cyclones.

TSSN is presently defined as concurrent surface observations of snowfall and lightning (Schultz 1999). Previous literature studied TSSN with Meteorological Terminal Air Report (METAR) observations (e.g., Market et al. 2002), or ground-based lightning networks (Pettegrew 2008; Kumjian and Deierling 2015; Schultz et al. 2018). Market et al. (2002) developed a METAR-based climatology and found that the Intermountain West, Great Lakes, and Great Plains were areas where TSSN was most frequently observed. The Market et al. (2002) climatology was limited due to subjective identification problems; for example, if lightning occurred nearby according to a lightning detection network, and a trained weather observer observed snowfall at the station location, a TSSN tag would not be inserted into the METAR unless lightning/thunder

was physically witnessed by the observer (Department of Commerce 2017). However, as Kumjian and Deierling (2015) discuss, this climatology may be under representing TSSN observations because they observed more frequent TSSN events on the Colorado Front Range than the Market et al. (2002) study. Furthermore, Kumjian and Deierling (2015) state that one of these TSSN flashes along the Colorado Front Range was triggered by a tower.

Tall human-made structures have been known to be an initiation point for cloud-to-ground (CG) lightning. Kingfield et al. (2017) demonstrated a positive correlation with tower height and CG occurrence and found that towers taller than 400 m above ground level experience an increase of CG lightning density by a median of 150% compared to surrounding areas. Furthermore, they suggest that shorter towers were more likely to be struck in the cold season as a result of charge centers being lower in winter storms. Rather than examining stationary towers, Montanya' et al. (2014) looked at lightning characteristics associated with wind turbines and found that the rotating blades of the wind turbines favored the occurrence of lightning. Tower-initiated flashes were only present on 0.3% of days when lightning occurred in Huntsville, AL between 2003 and 2015 (Schultz et al. 2019, accepted, pending revision). Tower-initiated flashes are more pronounced in winter because the tower can serve as a focusing mechanism that can directly interact with the main negative charge center (Schultz et al. 2019).

The environment for heavy-snowfall can be difficult to forecast owing to the mesoscale thermodynamic and microphysical processes within mid-latitude cyclones (Colle et al. 2014; Baxter and Schumacher 2017). High-resolution diagnostics of ingredients of heavy-snowfall beyond 12 hours are of limited values to forecasters, as the details of these forecasts will likely contain timing and placement errors (Evans and Jurewicz 2009). Therefore, forecasting heavy-

snowfall becomes a matter of nowcasting and increasing situational awareness rather than being predictive in nature (Wiesmueller 1998). The ability to objectively identify lightning by GLM that occurs while snow is falling at the surface will lead to further understanding of thermodynamic and microphysical processes in mid-latitude cyclones because the GLM flash size is fundamentally controlled by these processes (Saunders et al. 2006, Bruning and MacGorman 2013). Thus, the characterization of atmospheric profiles in which lightning develops provides the potential for development of innovative products tailored to increasing situational awareness of high impact events. The quantification of the ranges in flash sizes and total optical energies in TSSN events have been very limited due to the lack of geostationary observations of lightning from GLM prior to 2017; therefore, the objectives of this work are to:

1) Characterize and quantify the ability of the GOES-East GLM instrument to detect and observe TSSN events compared to previous studies,

2) Statistically analyze the GLM flash characteristics of duration, area, and total optical energy, and place them in the context of lightning within other regions of mid-latitude cyclones not producing snowfall, and

3) Compare and contrast GLM to ground-based lightning network observations of TSSN to understand the capability of GLM compared to current sensors.

2. Datasets

a. Geostationary Lightning Mapper

GLM is an optically based instrument that has a hemispheric field-of-view between 52°N/S with a near-uniform spatial resolution of 8 km. GLM detects light in a narrow 1 nm band centered on the 777.4 nm wavelength (Christian and Goodman 1987; Goodman et al. 2013;

Rudlosky et al. 2019). This particular wavelength allows GLM to observe lightning both during the day and at night. There are three basic components that GLM provides: events, groups, and flashes (Goodman et al. 2013). An event is when a single pixel in the GLM field-of-view becomes more illuminated than a background threshold. A GLM group is one or more events in a single frame that occur adjacent to each other. A GLM flash is presently defined as a set of groups within a weighted Euclidean distance bounded by 330 ms/16.5 km (Goodman et al. 2013). Each GLM flash contains information on the area of the flash (km^2) and its total optical energy output (femtojoule; fJ). Additionally, GLM is designed to have a total lightning detection efficiency (i.e., probability of detection, POD) of at least 70% with 5% false alarms. For a full description of GLM specs and capabilities see Goodman et al. (2013). Level 2 GLM data utilized in this study was from the GOES-R Calibration/Validation (Cal/Val) Group.

b. National Lightning Detection Network

In contrast to GLM, the National Lightning Detection Network (NLDN; Cummins and Murphy 2009) does not detect lightning optically from space but rather is a system of ground-based sensors that can detect electromagnetic signals radiated by lightning. Unlike GLM, NLDN has the capacity to differentiate lightning flashes as CG or intracloud (IC) and can detect CG and IC flashes with a detection efficiency of 90-95% and 50-60% respectively (Cummins and Murphy 2009; Murphy and Nag 2015). Recent upgrades have improved the detection of IC flash information and provided IC flash multiplicity and connected IC flash information with CG flash locations (Murphy and Nag 2015). The point flash locations of the NLDN data provides information about lightning characteristics during flash propagation that cannot be determined by examining GLM data alone (e.g., is the flash in the cloud or connecting to the ground).

Currently, NLDN defines a flash as a grouping of CG strokes and/or cloud pulses that are bounded by 500 ms/10 km (Cummins et al. 1998; Murphy and Nag 2015).

c. Merged Snowfall Rate product

National Environmental Satellite Data and Information Service (NESDIS) merged Snowfall Rate (mSFR; Meng et al. 2017a,b) product is a blended product using passive microwave sensors and the Multi-Radar Multi-Sensor (MRMS; Zhang et al. 2016) to estimate snowfall rates. The passive microwave sensors used to develop the mSFR product are the: Advanced Microwave Sounding Unit (AMSU), Microwave Humidity Sounder (MHS), Advanced Technology Microwave Sounder (ATMS), Special Sensor Microwave Imager/Sounder (SSMIS), and Global Precipitation Measurement (GPM; Hou et al. 2014; Skofronick-Jackson et al. 2017) Microwave Imager (GMI). The use of passive microwave sensors have been shown to estimate snowfall rates prior to snowfall reaching the surface (Meng et al. 2017b, Ferraro et al. 2018) and the MRMS portion fills in the gap between satellite overpasses with a spatio-temporal resolution of 1x1 km and 10 minutes and provides continuous coverage for the CONUS. The snowfall rates from MRMS are precipitation rates at the surface associated with the "snow" precipitation flag (Huan Meng, NESDIS, personal communication). Furthermore, the MRMS defines precipitation falling as snow when the surface temperature and wet-bulb temperature are below 2°C and 0°C respectively (Zhang et al. 2016). The mSFR was utilized in conjunction with GLM to identify TSSN. In this study, TSSN was defined as lightning, observed from GLM, which simultaneously occurred in an area where the MRMS portion of the mSFR product depicted snowfall; the objective identification process will be described in more detail in section three.

d. Tall Human-made Structures

Data from the Homeland Infrastructure Foundation-Level Data (HIFLD; Homeland Infrastructure Foundation-Level Data cited 2019) and the U.S. Wind Turbine Database (USWTDB; Hoen et al. 2018) were collected. Specifically, the cellular towers and antenna structure registration datasets in the HIFLD were collected. The cellular towers dataset consists of cellular tower locations that are recorded by the Federal Communications Commission (N=23,498) and the antenna structure registration contains antenna structure that are more than 60.96 m (200 feet) tall or antenna near airports (N=124,811). Furthermore, the USWTDB dataset contains the locations of 58,449 wind turbines within 43 states. Combined, these datasets provide locations where tall human-made object initiated TSSN may occur in the CONUS. A complete tall human-made structure dataset does not currently exist for tower locations in Canada; therefore, potential tower locations in Canada were subjectively identified using Google Earth imagery.

3. Methodology

a. TDA Objective Identification

The domain of interest was from 23°N to 50°N latitude and from 110°W to 65°W longitude. Snowfall cases were collected based on snowfall accumulation potential rather than snowfall cases that were associated with TSSN. Potential cases were determined by examining National Weather Service (NWS) forecast discussions and numerical weather prediction output. Forecast discussions were automatically scanned for keywords (i.e., snowfall, frontogenesis, etc.) to identify geographic locations that would experience heavy-snowfall in the near-future. Cases

were not collected prior to January 2018 given that GLM was still in the checkout phase and had not reached a provisional status (National Oceanic and Atmospheric Administration 2018).

Using the mSFR product, Level 2 GLM data, and nearest neighbor statistics (Bentley 1975), a thundersnow detection algorithm (TDA) was developed. Figure 1 demonstrates a flow chart of TSSN flash identification process within the TDA. The TDA utilized GLM groups rather than GLM events as it was computationally inexpensive compared to using events. Additionally, GLM groups provide more spatial information than a single GLM flash centroid coordinate and resulted in an increased likelihood of classifying TSSN. The first step of the TDA involved binning the GLM groups every 10 minutes to match the temporal resolution of the mSFR product. For example, if the mSFR product timestamp was 1030 UTC, the GLM groups were binned from 1030-1039 UTC. By using nearest neighbor statistics, step two involved the objective identification of the overlap between mSFR and GLM data. Nearest neighbor statistics were used to mitigate parallax issues within the GLM data and potential scattering effects in the mSFR product. The MRMS input of the mSFR product exploits higher resolutions compared to the passive microwave portion; thus, the examination between GLM and the mSFR product was based on the MRMS portion. In step three, a maximum distance threshold of 0.15 degrees was used to find mSFR pixels near a single GLM group. A distance of 0.15 degrees is approximately 16.6 km (roughly the same distance used to create an official GLM flash; Goodman et al. 2013). A confidence level for lightning flashes observed by GLM that occurred in snowfall was assigned based on the number of mSFR pixels that were identified as snow in the 16.6 km search area (see Fig. 1 for an example). The higher the mSFR pixel count within the maximum distance threshold, the higher the confidence the GLM group could be classified as a GLM group associated with snowfall. Figure 1

showcases the nearest neighbor statistics with regards to a single GLM group associated with snowfall with low confidence (mSFR pixel count of 4). Furthermore, if a GLM group had no mSFR pixels within the maximum distance threshold it would be classified as a GLM group not associated with snowfall. The classification process continued until all GLM groups were classified as TSSN or non-TSSN. Using GLM flash characteristics (i.e., flash ID, flash start/end times) and the mSFR timestamp, the fourth and last major step of the TDA is matching up the TSSN classified GLM group data to the official GLM flash data. This reduces the amount of data to be processed and simplifies further analysis. Additionally, the confidence level of these flashes being classified as TSSN became the average mSFR pixel count from the GLM groups that make up a GLM flash. For example, if a GLM flash was made up of three GLM groups and had mSFR pixel counts of 700, 565, and 865 the confidence level of the GLM flash would be 710. The TDA then removes duplicate GLM flashes as some snowfall cases overall with each other. This matchup process was necessary as it allowed for analysis regarding official GLM flash variables (e.g., flash area) while still maintaining the characteristics of the lightning when associated with snowfall (i.e., average mSFR pixel count).

All GLM flashes that were identified by the TDA were classified as potential TSSN and were binned every 25 mSFR pixel count (i.e., 0, 25, 50, etc.); meaning that the 25 mSFR confidence bin contained all potential TSSN flashes identified by GLM that have a mSFR pixel count of 25 or greater. This allowed for statistical analysis between the different confidence bins. Even though the mSFR pixel count can exceed 860 (i.e., area of distance threshold ($\pi*16.6^2$)), the highest mSFR confidence bin was set as 825 because of the need to have enough GLM flashes within the bin for any statistical comparison. TSSN flashes observed by GLM were assumed to have similar GLM

213 characteristics with regards to flash energy and flash area. Therefore, the flash characteristics
214 (i.e., flash energy and area) for GLM flashes within the highest mSFR confidence bin (i.e., GLM
215 flashes with a mSFR pixel count ≥ 825) were compared to GLM flash characteristics in different
216 mSFR confidence bins to determine whether they could be considered statistically similar (i.e., p-
217 value). The GLM flashes within the highest number mSFR confidence bin that did not exhibit
218 statistically significant differences (i.e., $p>0.01$) compared to the highest mSFR confidence bin
219 were objectively classified as TSSN. The 0.01 significance level was used compared to the $p=0.05$
220 to increase the number of objective classification of TSSN. As a proof of concept of the TDA
221 process, Fig. 2a illustrates a 10 minute bin of GLM group (black dots) data overlapping with mSFR
222 product data in southern Minnesota and northern Iowa. The GLM groups in central Iowa were
223 not overlapping any mSFR data and therefore were classified as non-TSSN groups. In contrast,
224 Fig. 2b depicts GLM flashes for the same timeframe and illustrates the effectiveness of the TDA
225 framework for disregarding GLM groups that were not overlapped with the mSFR product. This
226 demonstrates that the TDA can objectively identify the overlapping of the mSFR product and GLM
227 dataset and thus creates a reliable and robust way of identifying TSSN.

228 *b. NLDN/GLM Matchup and Classification*

229 TSSN flashes observed by GLM were matched up with NLDN flashes to further quantify
230 TSSN. Given that the GLM and NLDN flash locations are point locations, the datasets were
231 matched up based on the timing and spatial footprint characteristics of a GLM flash. To be initially
232 assigned to a GLM flash, a NLDN flash must occur within a ±1 second time buffer outside of the
233 start and end time of a GLM flash. Two distance thresholds (i.e., 50 km and the square root of
234 GLM flash area) were used in the spatial matchup process to account for diverse GLM flash

area/spatial footprints. For a NLDN flash to spatially match a GLM flash, the great-circle distance between a GLM flash centroid coordinate and NLDN flash location must be less than the larger of the two distance thresholds (50 km or square root of GLM flash area). The use of the 50 km distance threshold accounted for small elliptical GLM flashes that were not well represented by the square root of the GLM flash area. The use of the spatial footprint, rather than the centroid coordinate, of a GLM flash allowed for a greater possibility to matchup GLM and NLDN. Additionally, the spatial footprint was also used given multiple NLDN flashes can coincide in space and time with a single GLM flash because the NLDN data do not contain information on the spatial extent of lightning (Schultz et al. 2018).

Finally, the NLDN CG flash coordinates that matchup with the TSSN flashes observed by GLM were used to determine whether the GLM flash could be associated with a tall human-made object. Given the NLDN flash data has a median spatial error of 500 m (Cummins and Murphy 2009), a 500 m buffer was created around the tall human-made structures in the HIFLD and USWTDB datasets and determined which NLDN CG flashes occur in that buffer region and those that do not. The NLDN CG flashes that did occur in that buffer were classified as tower flashes and the remaining NLDN CG flashes within the CONUS were classified as non-tower flashes. The NLDN CG flashes that occurred in Canada were classified as tower and non-tower based on Google Earth imagery because of the lack of tower related dataset. The TSSN flashes observed by GLM were then classified as: IC-only, tower, non-tower and no NLDN. IC-only TSSN flashes detected by GLM were those that only contain NLDN IC flashes. The tower and non-tower TSSN flashes observed by GLM were associated with at least one NLDN CG flash and the specific CG type classification was based on the timing of the first CG occurrence. For example, if a GLM flash

had two NLDN CGs associated with it (one tower and one non-tower) and the first CG that occurred was classified as non-tower (i.e., occurring outside any 500 m buffer) the GLM flash would be classified as a non-tower TSSN flash. In contrast, GLM flashes that did not matchup with any NLDN data were classified as "no NLDN" as there was no way to classify the flashes as IC or CG with certainty.

4. Results

a. Objective Identification

A total of 21 heavy-snowfall cases that occurred from January-April 2018 were identified, with 20 of them producing at least one lightning flash during snowfall, cases numbered 1 to 21 are listed in Table 1. Twenty of the 21 snowfall cases produced a total of 51,397 potential TSSN flashes observed by GLM (i.e., GLM flashes with a mSFR pixel count > 0). The snowfall cases ranged from convective snowfall in Oklahoma and Texas, to heavy-snowfall in the Great Plains and Midwest regions to Nor'easters along the East Coast. Of the 21 collected cases, 8-10 and 21 made up 89.5% of the TDA identified potential TSSN flashes with approximately 74.8% of them being from cases 8-10 (Table 1). It should be noted that cases 8-10, which occurred in Texas, Oklahoma, and Kansas were convective snowfall cases that produced little to no snowfall accumulation. The GLM flashes that occurred during these cases were not associated with a mid-latitude cyclone, but were rather associated with an influx of moisture from the Gulf of Mexico resulting from a strong cold front propagating from northwest to southeast. The case that produced the most potential TSSN flashes detected by GLM (N=7,562), with snowfall accumulation, was the 13-17 April 2018 blizzard (case 21; Table 1).

b. GLM Characteristics

Mann-Whitney-Wilcoxon two-sided test was used to compare GLM flash area and flash energy of the lower mSFR confidence bins (i.e., 0, 25, 50, etc.) to the highest mSFR confidence bin of 825 to determine the appropriate bin for TSSN classification. In other words, how many mSFR pixels need to be associated with a GLM flash to confidently classify it as TSSN? Compared to the GLM flashes within the highest mSFR confidence bin, the GLM flashes within the 700 mSFR confidence bin were not statistically different at the 0.01 significance level with a p-value of 0.101 and 0.048 for GLM flash area and flash energy respectively which represent z-scores of 1.28 and 1.66 (Table 2); therefore, the GLM flashes within the 700 mSFR confidence bin could be objectively classified as TSSN at the 0.01 significance level. GLM flashes within the 700 mSFR confidence bin have over 80% of the mSFR pixels classified as snow and exhibit similar flash area and energy characteristics compared to GLM flashes within the 825 mSFR confidence bin which were characterized as approximately 95% of mSFR pixels classified as snow. Furthermore, when examining flash energy, GLM flashes within the 675 mSFR confidence bin and lower were statistically different ($p<0.01$) compared to the GLM flashes within the 825 mSFR confidence bin (Table 2) and have less than 80% of the mSFR pixels classified as snow; therefore, these GLM flashes could not be objectively classified as TSSN at the 0.01 significance level. This resulted in 2,214 of the 51,397 TDA identified GLM flashes as being objectively classified as TSSN. Table 2 contains GLM flash energy and flash area statistics for various mSFR confidence bins and demonstrates that as the mSFR count increases both flash energy and area increase. TSSN flashes observed by GLM (i.e., GLM flashes with a mSFR pixel count ≥ 700) had a mean flash area and flash energy of 754 km^2 and 1,342 fJ respectively (Table 3) and the mean duration of TSSN flashes

identified by GLM was 402 ms with a maximum duration of 2,718 ms. Table 3 contains flash area, energy, and duration statistics and demonstrates that TSSN flashes observed by GLM have some degree of variability. For example, a TSSN flash observed by GLM that occurred at 02:32:33 UTC on 14 April 2018 had the largest flash area (5,010 km^2). Similarly, the largest TSSN flash detected by GLM also had the highest GLM flash energy value (28,890 fJ) and a shorter than average flash duration of 344 ms. The longest duration flash occurred at 18:23:24 UTC on 13 April 2018 and had a flash area and flash energy of 1,779 km^2 and 8,233 fJ respectively. Additionally, it was found that GLM flash energy was more correlated with flash area (e.g., Pearson correlation of 0.77) than flash duration (e.g., Pearson correlation of 0.43). Figure 3 illustrates that GLM flash size and flash energy of cases associated with snowfall (orange dots; TSSN flashes) are on the upper end of the flash energy per flash area spectrum. TSSN events demonstrate less variability in the flash energy per flash area spectrum and the relationship between flash area and flash energy is more defined compared to the potential TSSN events. The lack of variability for TSSN flashes compared to potential TSSN flashes observed by GLM suggest microphysical and thermodynamic differences exists between the two classifications; however, an in-depth analysis is beyond the scope of this study.

c. NLDN and GLM Intercomparison

The 2,214 TSSN flashes observed by GLM were matched with ground-based NLDN data. When using the one second time buffer and spatial matchup parameters, it was found that 1,709 TSSN flashes identified by GLM corresponded with at least one NLDN flash (i.e., 77.2%). The median, mean, and maximum number of NLDN flashes to a GLM flash were 4.0, 5.9, and 37 respectively. Overall, there were 10,005 NLDN flashes that corresponded, spatially and

322 temporally, to 1,709 TSSN flashes identified by GLM. Of the 1,709 TSSN flashes observed by GLM
323 that had NLDN data correspondence, 1,129 of them were associated with at least one NLDN CG
324 flash. Furthermore, a comparison of flash area, energy, and duration for GLM flashes that
325 correspond to NLDN flashes (N=1,709) and those that did not correspond to a NLDN flash was
326 performed (N=505; Fig. 4). A random sample (N=505) of the GLM flashes that correspond to
327 NLDN was taken so that the two different datasets could be statistically compared. This resulted
328 in statically significant differences for GLM flash area, energy, and duration with p-values of
329 9.685×10^{-40}, 5.836×10^{-34}, and 8.296×10^{-13} respectively; suggesting that GLM was more likely to
330 identify flashes in snowfall that were on average spatially smaller with shorter flash durations
331 (Fig. 4a,c). Additionally, GLM flashes that were associated with CGs (i.e., tower and non-tower;
332 N=1,129) were on average spatially larger (1,013 vs. 572 km^2; Fig. 4a), contain more total optical
333 energy (2,098 vs. 732 fJ; Fig. 4b), and have a longer duration (476 vs. 358 ms; Fig. 4c) than IC-only
334 TSSN flashes identified by GLM (N=505). Figure 4 shows the flash area, energy, and duration
335 distributions for TSSN flashes identified by GLM that were categorized as tower, non-tower, and
336 IC-only flashes as well as the overall distributions of flashes associated with NLDN data and those
337 that were not. Next, the polarity and multiplicity of the 2,034 NLDN CG flashes that matched up
338 with GLM flashes were examined. Of the 2,034 NLDN CG flashes, 77.1% have a negative polarity
339 with a mean value of -14.71 kA (Table 4). The percentage of negative CGs in this study is
340 consistent with previous literature: 80% in Market and Becker (2009), 71% in Schultz et al. (2018),
341 and the 81% in Adhikari and Liu (2019) but is still lower than the 96% in Rauber et al. (2014) and
342 the 91% annual climatology in Orville and Huffines (2001). The cloud flash fraction of NLDN
343 flashes that matched up with GLM (i.e., the ratio of the number of NLDN ICs (N=7,971) to the

344 total number of NLDN flashes (N=10,005)) was found to be 0.80 and was comparable to the 0.79
345 for summer-time lightning in the Great Plains (Medici et al. 2017).

346 Using the USWTDB, HIFLD, and NLDN CG flash datasets, it was found that 246 tower and
347 883 non-tower TSSN flashes were detected by GLM. This resulted in 11.1% of the TSSN flashes
348 observed by GLM that matchup with NLDN as being associated with tall human-made structures.
349 Comparing tower (N=246) and non-tower (N=883) TSSN flashes observed by GLM revealed that
350 the flash area, energy, and duration were not statistically different with p-values of 0.504, 0.129,
351 and 0.915 respectively (Fig. 4a,b). A random sample of the NLDN non-tower CGs (N=1,713) was
352 used to compare those CGs with NLDN tower CGs (N=321). Using a random sample size of 321
353 non-tower CGs resulted in NLDN non-tower CGs having fewer return strokes on average
354 compared to NLDN tower CGs and were statistically significantly different ($p=4.99x10^{-10}$);
355 however, from a polarity perspective NLDN non-tower and tower CGs were not statistically
356 different (p=0.522). Table 4 contains the overall NLDN tower and non-tower CG multiplicity and
357 polarity characteristics. NLDN may be geographically limited compared to GLM's field-of-view
358 but can characterize lightning in greater detail; however, given that this study comprises a single
359 winter season, further study is needed to investigate the comparisons of TSSN and non-TSSN
360 flashes on a large scale.

361 *d. Spatial Distribution of TSSN from GLM*

362 The 21 cases from January-April 2018 can be compared directly with METAR reports to
363 understand the distribution of TSSN flashes over the CONUS (Fig. 5a). Figure 5a also
364 demonstrates the spatial distribution differences between TSSN flashes (mSFR pixel count ≥ 700**;**

orange dots) and potential TSSN flashes (mSFR pixel count > 0**;** blue dots) identified by GLM. The TSSN flashes observed by GLM suggests that TSSN was common throughout the Great Plains region in this study. During the date/times of interest, there were only 39 METAR reports containing TSSN (Fig. 5a; black dots) compared to 2,214 TSSN flashes observed by GLM; suggesting that TSSN was more common than indicated by previous literature and confirming limited identification in surface reports. Furthermore, gridding all potential TSSN flashes observed by GLM and plotting flash density resulted in a large area stretching from Texas to Minnesota that received elevated levels of TSSN flashes (Fig. 5b). The flash density was calculated using the potential TSSN flashes observed by GLM and binning them into 8 km bins to be consistent with the spatial resolution of the GLM and counting the number of flashes within each bin. The spatial distribution of the TSSN flashes (orange dots) match well with the gridded potential TSSN flashes observed by GLM and again demonstrates the idea that TSSN was more likely to occur in the Great Plains region compared to other geographic regions and is aligned with findings from previous literature (Market et al. 2002). It should also be noted that the TDA identified 122 potential TSSN flashes around and along the Lake Erie shoreline. Of those 122 potential TSSN flashes observed by GLM along Lake Erie, only 20 of them were classified as TSSN flashes. Given the timeframe of this study (January-April) and the climatological lake-air temperature difference is less compared to that in October-November, the TSSN flashes along the Great Lakes were more likely associated with lake-enhanced and not lake-effect snow (Harrington et al. 1987). This suggests further study is needed to demonstrate the ability of the TDA to identify TSSN in the early winter as lake-effect snow is more prominent (Steiger et al. 2009).

Contrasting the output of the TDA to METAR TSSN reports resulted in an extremely large false alarm rate (FAR); however, this was expected as the spatial and temporal coverage of GLM and mSFR are superior compared to METAR reports. Even though FAR was impractical in this study, the POD can still be calculated and was defined as:

$$POD = n\_GLM/n\_METAR$$

where *n_GLM* was the number of METAR TSSN reports that coincide with TSSN flashes observed by GLM and *n_METAR* was the total number of METAR TSSN reports. When comparing the METAR reports of TSSN to all GLM flashes that the TDA identified as being potential TSSN (N=51,397), the POD for this scenario was 66.7%. In contrast when examining all GLM flashes, not just those that were identified by the TDA, GLM detected lightning for 39 of those 39 METAR reports; thus the POD of TSSN, from a GLM perspective, was 100%. This suggests that the decrease of POD of TSSN from the TDA was a result of the mSFR product portion of the algorithm and represents one of the largest potential errors of the TDA. When examining the cases, the MRMS portion of the mSFR product sometimes "dropped" snowfall rates in some timeframes and came back in the next timeframe and was likely a result of how MRMS assigned the precipitation flag (Zhang et al. 2016; Meng et al. 2017b). This sporadic phenomena is likely associated with a rain/snow transition region (i.e., mixed precipitation types) and the mSFR product "drops" some snowfall rates due to classification issues between precipitation types within the MRMS (Steven Martinaitis, CIMMS/NSSL, personal communication). Regardless, with the advanced capabilities of GLM, identification of TSSN is robust and allows for expanded identification of the occurrence and spatial extent of TSSN compared to previous datasets.

5. Discussion

a. Comparison to Literature

The percentage of TSSN flashes involving towers in this study differs from Schultz et al. (2018) in which they found 11 of the 34 TSSN flashes were initiated from tall human-made objects. Even though this study contains more TSSN flashes, the discrepancy between these results were likely based on the locations in which the TSSN occur. The areas of interest in Schultz et al. (2018) were more heavily populated compared to this study, resulting in a higher density of tall-human made structures and was a likely reason why tower TSSN was more preferential. Additionally, the mean and maximum GLM flash area were spatially larger than the LMA-derived flash area in Schultz et al. (2018) (754 vs. 375 km^2 and 5,010 vs. 2,300 km^2 respectively). The large flash areas in this study were likely a result of: 1) how flash areas are determined based on very-high frequency (VHF) observations (i.e., LMA) compared to flash areas based on optical observations (i.e., GLM) and/or 2) LMAs limited range and lightning detection dropping off with distances exceeding 100 km from the network center (Fuchs et al. 2016; Koshak et al.2004).

Furthermore, the comparison of TSSN flash characteristics observed by GLM to the overall GLM flash characteristics is paramount to understanding the microphysical differences in lightning initiation between different environments. Rudlosky et al. (2019) demonstrated that, on average, GLM flashes over the ocean contained more total optical energy (420 vs. 230 fJ), were spatially larger (570 vs. 431 km^2), and have a longer duration (345 vs. 293 ms) compared to GLM flashes over land. In comparison, TSSN flashes detected by GLM on average contain more total optical energy (1,342 fJ), are spatially larger (754 km^2), and last longer (402 ms; Table 3). The mean flash energy metric falls between the 90^{th} and 99^{th} percentile of total flash energies

observed by GLM in Rudlosky et al. (2019) and were the reason behind the strong Pearson correlation of 0.77 between flash area and total flash energy. Thus, the flash properties in the present study can be placed into the context of the Bruning and MacGorman (2013) flash size spectra, and using knowledge from other studies that have examined the kinematic structure in mid-latitude cyclones (Rust et al. 2002, Rauber et al. 2014). It is speculated that the reason for the larger flash sizes and total optical energies observed in this study are due to the presence of broad, laminar mesoscale updrafts given that smaller flash sizes are typically associated with strong updrafts (≥ 10 m s^{-1}) in severe convection (e.g., Bruning and MacGorman 2013, Calhoun et al. 2013, Schultz et al. 2015; 2017).

b. Lack of Correspondence between GLM and the NLDN

Through the NLDN/GLM matchup process, 22.8% of GLM flashes did not correspond to any NLDN data. One possible explanation for the lack of NLDN/GLM correspondence was the GLM Lightning Cluster Filter Algorithm (LCFA) splitting spatially large and/or long duration TSSN flashes. If the GLM LCFA was splitting TSSN flashes, the end time of some GLM flashes would be the start time of other GLM flashes. If this phenomena happened and the GLM flash centroid coordinates were relatively close to each other provides evidence that the GLM LCFA was potentially splitting TSSN flashes. Using this methodology, it was found that 204 GLM flashes had start/end times the same as other flashes and eight of those flashes were not associated with NLDN flashes; furthermore using concurrent GLM start/end times, it was found that these 204 GLM flashes could be condensed down to 93 flashes with only three GLM flashes with no NLDN correspondence. Figure 6 demonstrates the GLM events (dots) associated with three GLM flashes (stars) to showcase the spatial proximity between them. The dashed circles represent the 50 km

search area in the NLDN/GLM matchup process for the individual GLM flashes; which resulted in 32 unique NLDN flashes (i.e., black plus symbols) in spatial and temporal proximity of the three GLM flashes. The solid lines represent the convex hull of the GLM flashes. These three GLM flashes sequentially occurred northwest of Sioux Falls, North Dakota at 21:09:37 UTC on 13 April 2018. The maximum great-circle distance between the first GLM flash centroid coordinate (red star) and the other two GLM flashes was 57.86 km. This suggests that the GLM LCFA split a single TSSN flash into three GLM flashes. The TSSN flash splitting from the GLM LCFA reduces the amount of GLM flashes with no NLDN data; however, this does not account for all GLM flashes that are not associated with NLDN flashes.

Given the fact that there were more NLDN IC flashes (N=7,971) compared to NLDN CG flashes (N=2,034), another possibility for the lack of GLM and NLDN correspondence was that NLDN was not detecting the TSSN because of the lower detection efficiency of IC flashes compared to CG flashes (Cummins and Murphy 2009; Murphy and Nag 2015). GLM flashes with no NLDN data (N=505) and GLM flashes that contain only ICs (N=580) were statistically different when examining GLM flash area, energy, and duration ($p<0.01$) with p-values of 7.845×10^{-17}, 1.315×10^{-18}, and 2.077×10^{-6} respectively. The p-values when comparing the GLM flashes with no NLDN and those that contain at least one CG (N=1,129) were 1.265×10^{-84}, 1.612×10^{-67}, and 2.927×10^{-24} for flash area, energy, and duration respectively. Through these comparisons it is reasonable to assume that the GLM flashes with no NLDN data are statistically more likely to be IC-only flashes than flashes with at least one CG. Thus, suggesting that NLDN was not detecting TSSN ICs that GLM could detect. This again provides evidence that GLM and ground-based lightning data need to be used in tandem to characterize TSSN.

c. Future Improvements to the TDA

In this study, the MRMS portion of the mSFR product was exclusively used to detect TSSN. The opportunity to extend the TDA to incorporate passive microwave observations to discriminate TSSN from non-TSSN (e.g., Adhikari and Liu 2019) provides value to areas outside the CONUS. The main challenge will be that these products detect snowfall falling aloft and near the surface and the current passive microwave part of the mSFR product can only detect snow in regions that are warmer than -14°C/7°F (Meng et al. 2017a). Even with this limitation, this portion of the mSFR product provides valuable insight in data sparse regions and can be matched up with other lightning sensors to classify lightning as potential TSSN to understand the microphysical processes associated with the development of TSSN from a space-based remote sensing perspective. The implementation of a TDA-like algorithm towards these sensors and other lightning datasets would provide the first objective TSSN detection using passive microwave sensors and would provide global coverage; however, greater spatial and temporal sampling is needed for such an implementation.

6. Conclusion

Previous studies have subjectively identified TSSN; however, the TDA allowed for the objective identification of this phenomena by utilizing GLM, the mSFR product (i.e., MRMS data), and nearest neighbor statistics. Snowfall cases were collected from January-April 2018 and a TDA was developed to quantify the ability of GLM to identify TSSN events and resulted in the identification of 51,397 potential TSSN flashes. The degree of confidence of a GLM flash being classified as TSSN was determined by the average mSFR pixel count and GLM flashes with a mSFR

pixel count greater than or equal to 700 were objectively classified as TSSN (N=2,214). Utilizing METAR reports of TSSN as truth, the TDA identified TSSN with a POD of 66.7%. The TDA process also reiterates that TSSN was more likely to occur in the Great Plains, Intermountain West, and Great Lakes regions and was comparable to previous literature (i.e., Schultz 1999; Market et al. 2002). Compared to GLM flash characteristics in Rudlosky et al. (2019), TSSN flashes observed by GLM were found to be spatially larger, contain more total energy, and have a longer duration than non-TSSN flashes over land and ocean.

Of the 2,214 TSSN flashes observed by GLM, 1,709 of them correspond spatially and temporally to NLDN and were classified as IC-only (N=580), tower (N=246), and non-tower (N=883). This corresponds to 11.1% of TSSN flashes observed by GLM being associated with tall human-built objects like antenna or wind turbines. Furthermore, when comparing GLM flashes that matched up with NLDN to those that do not resulted in statistically significant differences for GLM flash area ($p=9.685x10^{-40}$) and flash energy ($p=5.836x10^{-34}$); suggesting that GLM was more likely to identify spatially smaller lightning flashes within snowfall. Nearly 23% of GLM flashes did not matchup with any NLDN flashes and was likely caused by: 1) TSSN flash splitting by the GLM LCFA and/or 2) the lower detection efficiency of ICs from NLDN. Several instances of GLM TSSN flash splitting were found (see Fig. 6 for an example) but does not completely account for the lack of NLDN/GLM correspondence. It was found that TSSN flashes detected by GLM without NLDN correspondence were statistically more likely to be classified as IC-only compared to GLM flashes associated with at least one CG; suggesting, NLDN was not detecting ICs that GLM can detect. Overall, this study expands upon previous research by objectively identifying TSSN by utilizing next-generation satellite sensors and derived products; providing the first steps to

517 characterize TSSN from a GLM perspective. Future work includes characterizing TSSN on a large
518 scale from a thermodynamic and microphysical aspect.

519

520 *Acknowledgments.* This work was directly supported by Dr. Tsengdar Lee of NASA's Research and
521 Analysis Program, Weather Focus Area, as part of the Short-term Prediction Research and
522 Transition (SPoRT) Center at Marshall Space Flight Center. This work was also supported through
523 the NASA-UAH Cooperative agreement # NNM11AA01A. The authors wish to thank Dr. Geoffrey
524 Stano of UAH for providing support for all things GLM, Dr. Huan Meng of NESDIS for providing
525 the mSFR product data, and Vaisala for providing the NLDN data. The authors would also like to
526 thank Drs. Kevin Knupp and John Mecikalski of UAH for their continued support. Additionally, the
527 authors would like to thank Samantha Edinton and Clem Tillier of Lockheed Martin for providing
528 the GLM Cal/Val data and Doug Mach for processing the data into flashes. The authors would
529 also like to thank the three anonymous reviewers for providing valuable insight and suggestions.

530 **References**

531 Adhikari, A., and C. Liu, 2019: Geographic distribution of thundersnow events and their properties
532 from GPM Ku-band radar. *J. Geophys. Res. Atmos.*, **124**, doi:10.1029/2018JD028839.
533 Baxter, M. A., and P. N. Schumacher, 2017: Distribution of Single-Banded Snowfall in Central
534 U.S. Cyclones. *Wea. Forecasting*, **32**, 533–554, doi:10.1175/WAF-D-16-0154.1.
535 Bentley, J. L., 1975: Multidimensional Binary Search Trees Used for Associative Searching.
536 *Communications of the ACM*, **18**(9), 509–517, doi:10.1145/361002.361007.
537 Bruning, E. C., and D. R. MacGorman, 2013: Theory and Observations of Controls on Lightning
538 Flash Size Spectra. *J. Atmo. Sci.*, **70**(12), 4012–4029, doi:10.1175/JAS-D-12-0289.1.
539 Calhoun, K. M., D. R. MacGorman, C. L. Ziegler, and M. I. Biggerstaff, 2013: Evolution of lightning
540 activity and storm charge relative to dual-Doppler analysis of a high-precipitation

supercell storm. *Mon. Wea. Rev.*, **141**, 2199-2223, doi:10.1175/MWR-D-12-00258.1.

Christian, H. J., and S. J. Goodman, 1987: Optical observations of lightning from a high altitude airplane. *J. Atmos. Oceanic Technol*., **4**, 701–711, doi:10.1175/1520-0426(1987)004<0701%3AOOOLFA>2.0.CO%3B2.

Colle, B. A., D. Stark, and S. E. Yuter, 2014: Surface Microphysical Observations within East Coast Winter Storms on Long Island. *Mon. Wea. Rev.*, **142**, 3126–3146, doi:10.1175/MWR-D-14-00035.1.

Cummins, K. L., and M. J. Murphy, 2009: An overview of lightning locations systems: History, techniques, and data uses with an in-depth look at the U.S. NLDN. *IEEE Transactions on Electromagnetic Compatibility*, **51**(3), 499–518, doi:10.1109/TEMC.2009.2023450.

Department of Commerce, 2017: Federal Meteorological Handbook No. 1 Surface Weather Observations and Reports. [Available online at: https://www.ofcm.gov/publications/fmh/FMH1/FMH12017.pdf].

Evans, M., and M. L. Jurewicz, 2009: Correlations between Analyses and Forecasts of Banded Heavy Snow Ingredients and Observed Snowfall. *Wea. Forecasting*, **24**, 337–350, doi:10.1175/2008WAF2007105.1.

Ferraro, R., and Coauthors, 2018: Snowfall rates from satellite data help weather forecasters. *Eos*, **99**, doi:10.1029/2018EO096715.

Fuchs, B. R., E. C. Bruning, S. A. Rutledge, L. D. Carey, P. R. Krehbiel, and W. Rison, 2016: Climatological analyses of LMA data with an open-source lightning flash clustering algorithm. *J. Geophys. Res. Atmos.*, **121**, 8625–8648, doi:10.1002/2015JD024663.

Goodman, S. J., and Coauthors, 2013: The GOES-R Geostationary Lightning Mapper (GLM). *Atmo. Res.*, **125-126**, 34–49, doi:10.1016/j.atmosres.2013.01.006.

Harrington, J. A., Jr., R. S. Cerveny, and K. F. Dewey, 1987: A Climatology of Mean Monthly Snowfall for the Conterminous United States: Temporal and Spatial Patterns. *J. Climate Appl. Meteor.*, **26**, 897–912, doi:10.1175/1520-0450(1987)026h0897%3AACOMMSi2.0.CO%3B2.

Hoen, B. D., J. E. Diffendorfer, J. T.Rand, L. A. Kramer, C. P. Garrity, and H. E. Hunt, 2018: United

States Wind Turbine Database. U.S. Geological Survey, American Wind Energy Association, and Lawrence Berkeley National Laboratory, Data Release: USWTDB V1.3 (January 7, 2019) [Available online at https://eerscmap.usgs.gov/uswtdb].

Homeland Infrastructure Foundation-Level Data, cited 2019: Homeland Infrastructure Foundation-Level Data (HIFLD). [Available online at: https://hifld-geoplatform.opendata.arcgis.com/datasets].

Hou, A. Y., and Coauthors, 2014: The global precipitation measurement mission. *Bull. Amer. Meteor. Soc.*, **95**, 701–722, doi:10.1175/BAMS-D-13-00164.1.

Kingfield, D. M., K. M. Calhoun, and K. D. de Beurs, 2017: Antenna structures and cloud-to-ground lightning location: 1995-2015. *Geophys. Res. Lett.*, **44**, 5203–5212, doi:10.1002/2017GL073449.

Koshak, W. J., R. J. Solakiewicz, R. J. Blakeslee, S. J. Goodman, H. J. Christian, and J. M. Hall, 2004: North Alabama Lightning Mapping Array (LMA): VHF source retrieval algorithm and error analysis. *J. Atmos. Oceanic Technol.*, **21**, 543–558, doi:10.1175/1520-0426(2004)021%3C0543:NALMAL%3E2.0.CO;2.

Kumjian, M. R., and W. Deierling, 2015: Analysis of Thundersnow Storms over Northern Colorado. *Wea. Forecasting*, **30**, 1469–1490, doi:10.1175/WAF-D-15-0007.1.

MacGorman, D. R., J. M. Straka, and C. L. Zeigler, 2001: A lightning parameterization for numerical cloud models. *J. Appl. Meteor.*, **40**, 459–478, doi:10.1175/1520-0450(2001)040h0459:ALPFNCi2.0.CO;2.

Market, P. S., and A. E. Becker, 2009: A study of lightning flashes attending periods of banded snowfall. *Geophys. Res. Lett.*, **36**, L01 809, doi:10.1029/2008GL036317.

Market, P. S., C. E. Halcomb, and R. L. Ebert, 2002: A Climatology of Thundersnow Events over the Contiguous United States. *Wea. Forecasting*, **17**, 1290–1295, doi:10.1175/1520-0434(2002) 017h1290:ACOTEOi2.0.CO;2.

Medici, G., 571 K. L. Cummins, D. J. Cecil, W. J. Koshak, and S. D. Rudlosky, 2017: The Intracloud Lightning Fraction in the Contiguous United States. *Mon. Wea. Rev.*, **145**, 4481–4499, doi:10.1175/MWR-D-16-0426.1.

Meng, H., J. Dong, R. Ferraro, B. Yan, L. Zhao, C. Kongoli, N. Y. Wang, and B. Zavodsky, 2017a: A 1DVAR-based snowfall rate retrieval algorithm for passive microwave radiometers. *J. Geophys. Res. Atmos.*, **122**, 6520–6540, doi:10.1002/2016JD026325.

Meng, H., E. Emily Berndt, and K. White, 2017b: NESDIS Snowfall Rate Product and Its Applications. JPSS Science Seminar, 20 November 2017, [Available online at: http://www.jpss.noaa.gov/assets/pdfs/science_seminars/presentations/SnowfallRate_Meng_White_Berndt_2017.pdf].

Montanya´, J., O. van der Velde, and E. R.Williams, 2014: Lightning discharges produced by wind turbine. *J. Geophys. Res. Atmos.*, **119**, 1455–1462, doi:10.1002/2013JD020225.

Murphy, M. J., and A. Nag, 2015: Cloud Lightning Performance and Climatology of the U.S. Based On The Upgraded U.S. National Lightning Detection Network. Extended Abstract, *Seventh Conf. on the Meteorological Applications of Lightning Data*, Phoenix, AZ, Amer. Meteor. Soc., [Available online at https://ams.confex.com/ams/95Annual/webprogram/Paper262391.html.].

National Oceanic and Atmospheric Administration, 2018: GOES-16 GLM Level 2 (Events, Groups, Flashes) Release, Provisional Data Quality. [Available online at: https://www.ncdc. noaa.gov/sites/default/files/attachments/ReadMe_GLM-LCFA_Provisional_Maturity.pdf].

Orville, R. E., and G. R. Huffines, 2001: Cloud-to-ground lightning in the United States: NLDN results in the first decade, 1989-98. *Mon. Wea. Rev.,* **139**, 2098–2109, doi:10.1175/1520-0493(2001)129h1179:CTGLITi2.0.CO;2.

Pettegrew, B. P., 2008: Analysis of Cloud and Cloud-to-Ground Lightning in Winter Convection. Ph.D. thesis, University of Missouri-Columbia, 223 pp., [Available online at: http://weather. missouri.edu/ROCS/pub/Pettegrew-Dissertation.pdf].

Rauber, R. M., and Coauthors, 2014: Stability and Charging Characteristics of the Comma Head Region of Continental Winter Cyclones. *J. Atmos. Sci.*, **71**, 1559–1582, doi:10.1175/JAS-D-13-0253.1.

Rudlosky, S. D., S. J. Goodman, K. S. Virts, and E. C. Bruning, 2019: Initial geostationary lightning

mapper observations. *Geophys. Res. Lett.*, **46**, 1097–1104, doi:10.1029/2018GL081052.

Rust, W. D., and R. J. Trapp, 2002: Initial balloon soundings of the electric field in winter nimbostratus clouds in the USA. *Geophys. Res. Lett.*, **29**, 1959, doi:10.1029/2002GL015278.

Schmit, T. J., M. M. Gunshor, W. P. Menzel, J. J. Gurka, J. Li, and A. S. Bachmeier, 2005: Introducing the Next-Generation Advanced Baseline Imager on GOES-R. *Bull. Amer. Meteor. Soc.*, **86**, 1079–1096, doi:10.1175/BAMS-86-8-1079.

Schultz, C. J., L. D. Carey, E. V. Schultz, and R. L. Blakeslee, 2015: Insight into the Kinematic and Microphysical Processes that Control Lightning Jumps. *Wea. Forecasting*, **30**, 1591-1621, doi:10.1175/WAF-D-14-00147.1

Schultz, C. J., L. D. Carey, E. V. Schultz, and R. L. Blakeslee, 2017: Kinematic and Microphysical Significance of Lightning Jumps versus Nonjump Increases in Total Flash Rate. *Wea. Forecasting*, **32**, 275-288, doi: 10.1175/WAF-D-15-0175.1.

Schultz, C. J., T. J. Lang, E. C. Bruning, K. M. Calhoun, S. Harkema, and N. Curtis, 2018: Characteristics of Lightning within Electrified Snowfall Events using Lightning Mapping Arrays. J*. Geophys. Res. Atmos.,* 1–21, doi:10.1002/2017JD027821.

Schultz, C. J., G. T. Stano, T. J. Lang, and P. M. Bitzer, 2019: Seasonal, Precipitation, and Electrical Attributes for Self-Initiated Lightning Events from Tall Structures in North Alabama. *Atmos. Res.*, accepted, pending revision.

Schultz, D. M., 1999: Lake-Effect Snowstorms in Northern Utah and Western New York with and without Lightning. *Wea. Forecasting*, **14**, 1023–1031.

Skofronick-Jackson, G, and Coauthors, 2017: The Global Precipitation Measurement (GPM) Mission for Science and Society. *Bull. Amer. Meteor. Soc.*, **98**(8), 1679-1695, doi: 10.1175/BAMS-D-15-00306.1.

Steiger, S. M., R. Hamilton, J. Keeler, and R. E. Orville, 2009: Lake-effect thunderstorms in the lower Great Lakes. *J. Climate Appl. Meteor.*, **48**, 889–902, doi:10.1175/2008JAMC1935.1.

Zhang, J., and Coauthors, 2016: Multi-Radar Multi-Sensor (MRMS) quantitative precipitation estimation: Initial operating capabilities. *Bull. Amer. Meteor. Soc.*, **97**, 621–638,

doi:10.1175/BAMS-D-14-00174.1.

TABLE 1. Snowfall cases from January-April 2018.

Case	Start date/time (UTC)	End date/time (UTC)	Classification	Number of potential TSSN flashes
1	2018-01-03 0000	2018-01-05 1500	Synoptic	37
2	2018-01-10 0000	2018-01-13 1700	Other	25
3	2018-01-21 0000	2018-01-23 2350	Synoptic	189
4	2018-02-06 0000	2018-02-08 0950	Synoptic	1,630
5	2018-02-08 0000	2018-02-10 2350	Other	1
6	2018-02-17 0000	2018-02-18 1450	Synoptic	1
7	2018-02-18 0000	2018-02-19 0550	Other	0
8	2018-02-19 0000	2018-02-21 1400	Other	18,978
9	2018-02-21 0000	2018-02-21 2350	Other	5,429
10	2018-02-22 0000	2018-02-22 2030	Other	14,023
11	2018-02-24 1000	2018-02-25 2350	Synoptic	21
12	2018-03-01 0000	2018-03-03 1440	Synoptic	31
13	2018-03-04 1900	2018-03-09 0950	Synoptic	1,300
14	2018-03-12 0000	2018-03-15 1550	Synoptic	21
15	2018-03-16 0600	2018-03-17 2210	Synoptic	996
16	2018-03-20 0000	2018-03-23 0550	Synoptic	35
17	2018-03-23 0600	2018-03-25 1150	Other/Synoptic	367
18	2018-03-30 0000	2018-03-31 2350	Synoptic	7
19	2018-03-31 1800	2018-04-02 1800	Other	528
20	2018-04-02 0600	2018-04-04 2359	Synoptic	216
21	2018-04-13 0000	2018-04-17 1620	Synoptic	7,562

694 TABLE 2. GLM flash area (energy) statistics with regards to mSFR count. Units of flash area and
695 energy are km^2 and (fJ; $1x10^{-15}$ J) respectively. Significance is relative to the GLM flashes within
696 the highest mSFR confidence bin (i.e., GLM flashes with a mSFR pixel count ≥ 825).

mSFR Count	Minimum	25th Percentile	Mean	Median	75th Percentile	Maximum	Significance (p-value)
0	67 (3.0)	228 (64)	607 (646)	428 (201)	755 (606)	8,735 (91,428)	1.315e-18 (1.135e-25)
100	67 (3.0)	228 (62)	600 (626)	429 (192)	758 (583)	5,911 (36,280)	2.630e-18 (2.222e-27)
200	67 (3.0)	226 (62)	599 (631)	429 (194)	755 (589)	5,911 (36,280)	2.864e-18 (6.336e-27)
300	67 (3.0)	232 (64)	607 (657)	434 (201)	773 (613)	5,911 (36,280)	2.886e-16 (9.300e-25)
400	67 (3.0)	277 (67)	616 (707)	439 (214)	787 (656)	5,588 (36,280)	2.599e-14 (2.509e-21)
500	67 (3.0)	282 (70)	634 (811)	443 (230)	812 (743)	5,121 (36,280)	1.767e-11 (1.7134e-16)
600	67 (3.0)	288 (82)	687 (1,022)	497 (290)	901 (1,004)	5,010 (36,280)	7.509e-06 (4.917e-08)
675	67 (3.0)	294 (96)	744 (1,265)	532 (371)	1,006 (1,340)	5,010 (28,890)	0.036 (0.009)
700	67 (3.0)	295 (96)	754 (1,342)	571 (382)	1,020 (1,452)	5,010 (28,890)	0.101 (0.048)
725	67 (6.0)	297 (105)	779 (1,459)	577 (435)	1,050 (1,550)	5,010 (28,890)	0.478 (0.364)
750	67 (6.0)	297 (105)	779 (1,476)	581 (435)	1,050 (1,671)	5,010 (28,890)	0.492 (0.486)
775	67 (6.0)	298 (107)	791 (1,531)	583 (449)	1,077 (1,760)	5,010(28,890)	0.818 (0.713)
800	67 (6.0)	298 (103)	783 (1,532)	581 (443)	1,054 (1,760)	5,010 (28,890)	0.594 (0.626)
825	67 (6.0)	326 (116)	785 (1,569)	590 (465)	1,072 (1,797)	3,260 (15,391)	1.000 (1.000)

697
698
699
700
701
702
703
704
705

706 TABLE 3. TSSN Flash Characteristics Observed by GLM (i.e., GLM flashes with a mSFR pixel count
707 ≥ 700).

Variable	25th Percentile	Mean	Median	75th Percentile	90th Percentile	99th Percentile
Area (km^2)	295	754	571	1,020	1,669	3,046
Energy (fJ)	96	1,342	382	1,452	3,853	11,874
Duration (ms)	162	402	329	562	830	1,608

708
709
710
711
712
713
714
715
716
717
718
719
720
721
722
723
724
725
726
727
728
729
730

731 TABLE 4. NLDN Multiplicity (number of return strokes) and Polarity (kA) Characteristics.

Variable	Type	Minimum	25th Percentile	Mean	Median	75th Percentile	Maximum
Polarity	All CGs	-621.30	-33.30	-14.71	-14.00	-4.52	327.50
	Tower CGs	-82.20	-20.70	-15.40	-13.90	-8.60	56.20
	Non-tower CGs	-621.30	-41.20	-14.58	-14.00	10.70	327.50
Multiplicity	All CGs	1.0	1.0	2.6	2.0	3.0	15.0
	Tower CGs	1.0	1.0	3.8	2.0	5.0	15.0
	Non-tower CGs	1.0	1.0	2.3	2.0	3.0	15.0

732
733
734
735
736
737
738
739
740
741
742
743
744
745
746
747
748
749
750
751
752
753
754

Figure 1

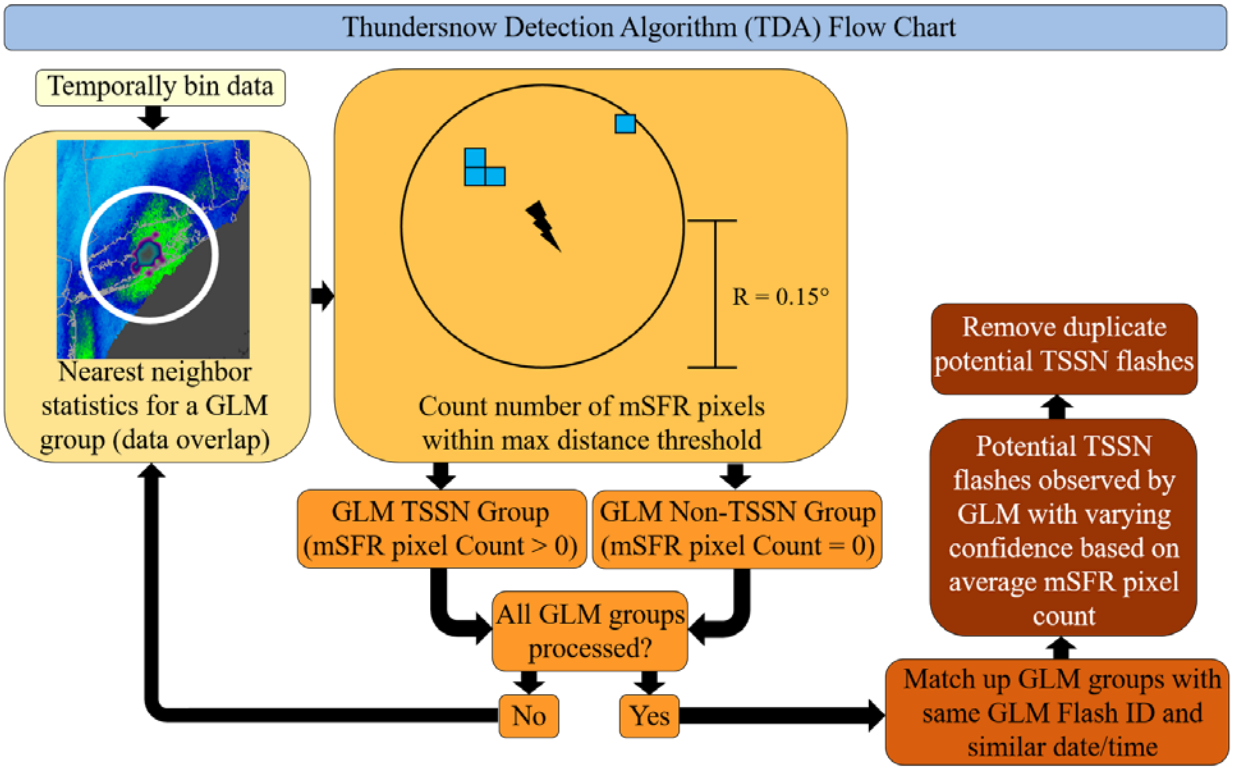

FIG. 1. Depiction of TDA processes associated with determination of TSSN flashes observed by GLM and confidences with the red hues getting darker as the TDA process proceeds. The black arrows represent the progressive steps of the algorithm. The first step involves binning the GLM data in 10 minute increments to match the temporal resolution of the mSFR product. If the mSFR product has a time stamp of 1010 UTC the GLM data would be binned from 1010-1019 UTC. Second step involves the overlap of mSFR and GLM data. For example, the mSFR (blues and greens) and GLM (in white circle) data within for a Nor'easter on 04 January 2018 at 1410 UTC over Long Island, New York displayed using the National Weather Service's Advanced Weather Interactive Processing System. The third step involves identification of TSSN groups observed by GLM based on a 0.15 degree distance threshold (black circle). Lightning bolt

represents a GLM group and the blue-filled boxes represent mSFR pixels. Pixel count equal to four results in a GLM group with low confidence of being TSSN. Step four is the GLM group classification based on number of mSFR pixels within distance threshold. If all GLM groups within that timeframe are process the TDA proceeds to step five and matches up the GLM groups by varies GLM flash characteristics to the official GLM flashes. Finally, the TDA removes duplicates as some cases are overlapped with each other.

Figure 2

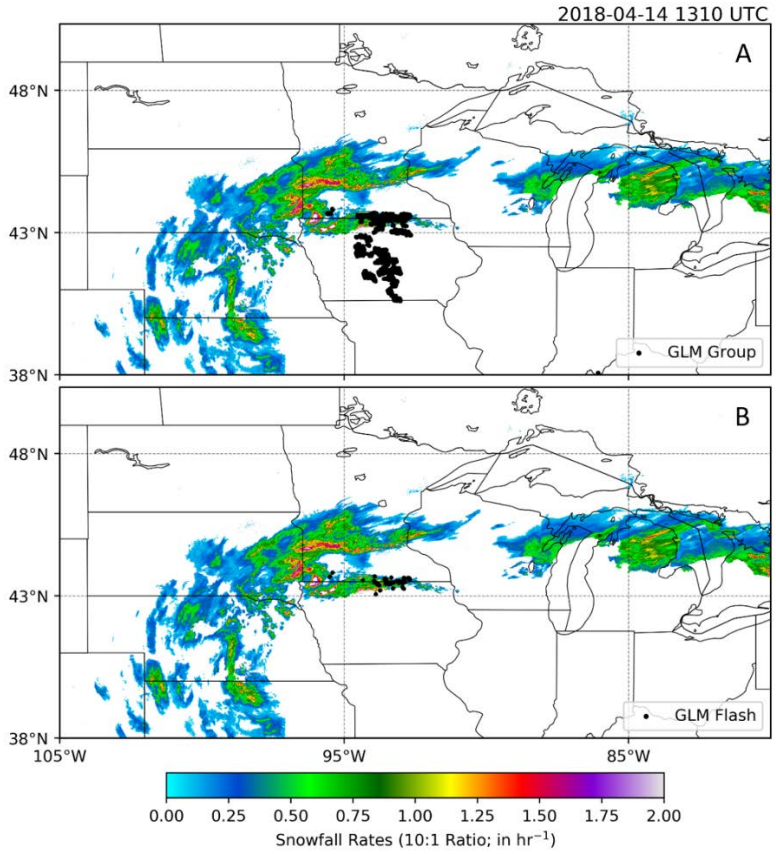

FIG. 2. 14 April 2018 1310 UTC NESDIS mSFR product overlaid with A) GLM group data and B) TSSN flashes observed by GLM from 1310 - 1319 UTC. This represents before and after the TDA takes effect respectively.

Figure 3

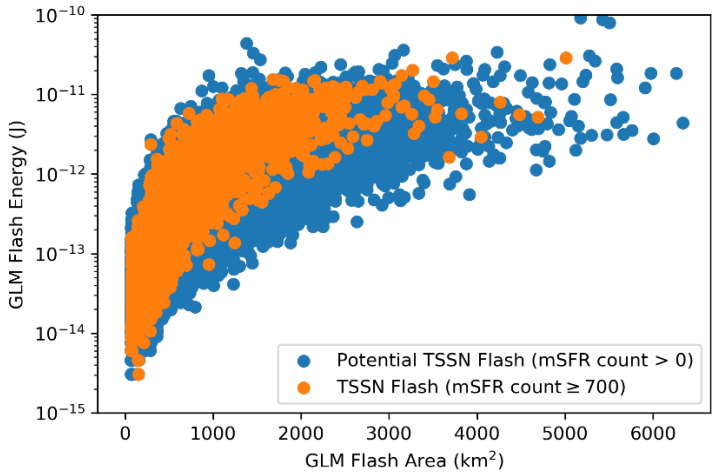

FIG. 3. Relationship between GLM flash energy and flash area. Blue represents all potential TSSN flashes observed by GLM and orange represents TSSN flashes observed by GLM with a mSFR count of 700 or greater.

Figure 4

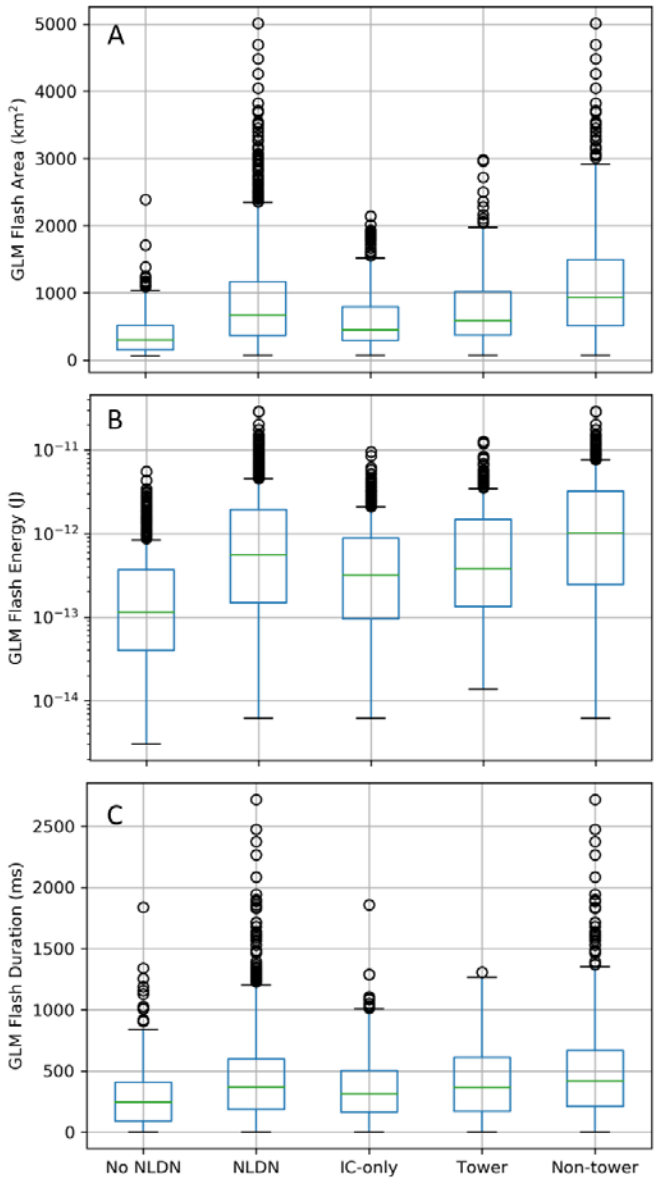

FIG. 4. Differentiation of GLM flashes with regards to flash: a) area, b) energy, and c) duration based on NLDN matchup characteristics. There is a total of 505 GLM flashes did not correspond with any NLDN data while the remaining 1,709 GLM flashes corresponded with NLDN data. The 1,709 GLM flashes subcategorized as IC-only (N=580), Tower (N=246) and Non-tower (N=883) initiated.

Figure 5

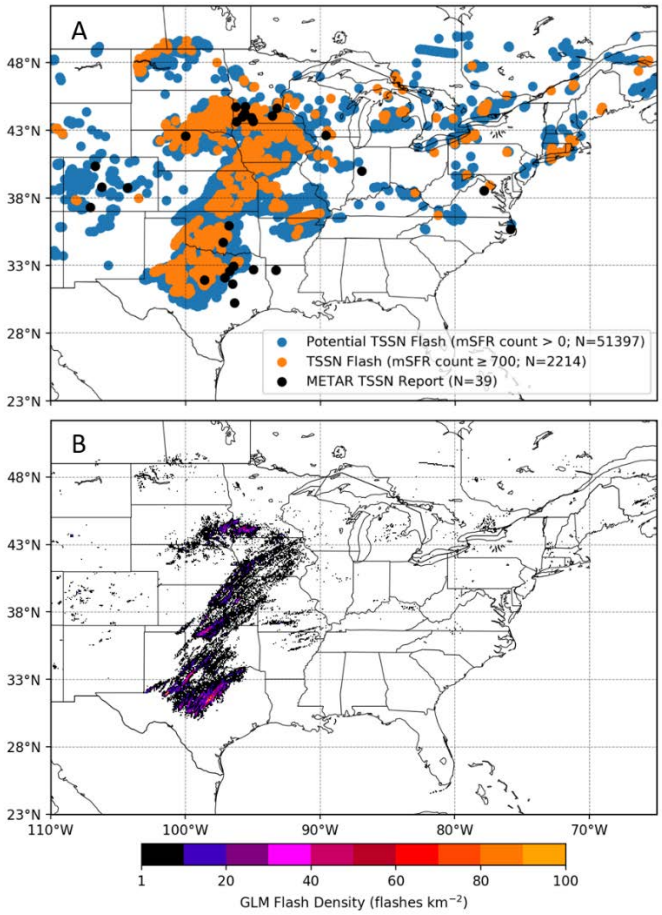

FIG. 5. A) Depicts flashes observed by GLM that occurred during the times in Table 1. Blue dots represent potential TSSN flashes observed by GLM; while orange dots represent TSSN flashes observed by GLM with a mSFR count of 700 or greater. Finally, the black dots represent METAR reported TSSN that occurred in the same range of time. B) Flash density for potential TSSN flashes detected from the TDA from January-April 2018.

841 **Figure 6**

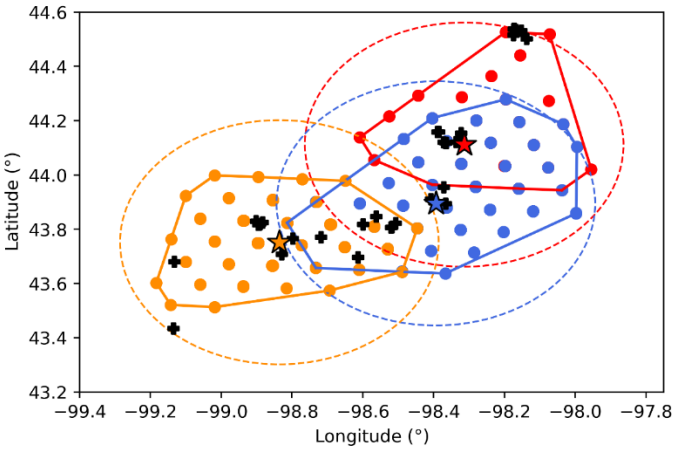

842

843 FIG. 6. Demonstration of the GLM LCFA splitting a TSSN flash into three separate GLM flashes

844 that occur sequentially northwest of Sioux Fall, North Dakota at 21:09:37 UTC on 13 April 2018.

845 Dots and stars represent GLM events and flashes respectively. The solid lines represent the

846 convex hull of the GLM flashes while the dashed line are the 50 km search radii in the

847 NLDN/GLM matchup process. The black plus represent the 32 unique NLDN flashes associated

848 with the three GLM flashes.